Asian Journal of Chemistry; Vol. 24, No. 4 (2012), 1554-1558

ASIAN JOURNAL OF CHEMISTRY

www.asianjournalofchemistry.co.in

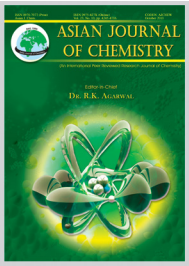

Influence of Synthesis on Constitution and Gas Sensing Property of SnO_2 Nanomaterial

XIAOMING MU, CHUANYUN PENG* and CHUNLAI WU

Department of Environmental and Chemical Engineering, Luoyang Institute of Science and Technology, Luoyang, Henan 471023, P.R. China

*Corresponding author: Tel: +86 0379 65928271; E-mail: chuanyunpeng@yahoo.cn

(*Received*: 5 March 2011; *Accepted*: 23 November 2011) AJC-10713

In this paper, nanostructure SnO_2 was prepared by dissolving tin granule in citric acid and gaining the precursor, which was treated with different ways and calcinated. The influence of treatment with the precursor on the gas sensing property of SnO_2 was studied. The precursor was treated with different methods and calcined at different temperature. SnO-doping SnO_2 was prepared from annealing the washed precursor and pure SnO_2 was synthesized from annealing the unwashed precursor. Four nanomaterials were obtained. The phases, constitution, morphology of them were characterized by XRD and SEM. Gas sensors were fabricated and an investigation into the SnO_2-based gas-sensing properties has been conducted. Compared to SnO-doping SnO_2, pure SnO_2 sensor shows much better gas sensing properties. It is more sensitive to H_2S, Cl_2, C_2H_5OH and HCHO than SnO-doping SnO_2.

Key Words: Tin dioxide, Precursor, Constitution, SnO-doping SnO_2, Sensitivity.

INTRODUCTION

Semi-conducting tin dioxide (SnO_2) is widely used as optoelectronic devices[1,2], gas sensors[3-5], dye-base solar cells[6], photocatalysts[7] and secondary lithium batteries electrode materials[8], because of its excellent photoelectric and chemical properties. Recently, SnO_2-based sensor has attracted increasing attention on gas sensing applications due to its suitable physico-chemical properties such as high stability, high reactivity to reducing gases at relatively low operating temperature. In particular, the synthesis of SnO_2 with particular conformation may provide promising gas-sensing performance. It is usually claimed that nanometer-scaled materials as gas sensors have significant advantages because of their small grain size, which becomes important to enhance the adsorption capacity. Control of the physical properties, such as film thickness, morphology, microstructure and stoichiometry of the elemental composition of the sensor layer, is vital as they determine the material's sensitivity and performance of the gas-sensing material. As discussed before, the physical properties are affected by the preparing methods. Nowadays, a great deal of work has been done on synthesizing sensing-materials such as sol-gel[9,10], chemical vapour deposition (CVD)[11,12] chemical precipitation[13-14], microwave digestion[15] and dissolution-pyrolysis[16]. Generally speaking, dissolution-pyrolysis is a simple way to synthesize SnO_2. SnO_2- based sensor fabricated by dissolution-pyrolysis method had fibrous microstructure, which could take finer effect on its gas sensing property[16].

In the present work, the precursor prepared through dissolution-pyrolysis is treated with different methods and calcined at different temperature. The constitution and micro-structure of the precursor is characterized in detail. The influence of different treatment of the precursor on the constitution, morphology and gas sensing properties of SnO_2 are investigated.

EXPERIMENTAL

All the chemical reagents used are analytical grade (Beijing Chemical Reagent Corp.). The preparation of SnO_2 was as follows: 4 g of metal tin and 80 g of citric acid were added in 100 mL of deionized water. After citric acid was completely dissolved by stirring, the reaction would last for 48 h at 175 ºC. Then cooling down to room temperature, the precipitated precursors on the bottom of flask were collected and separated into two portions leaving some to be characterized. One portion of it was pre-calcined at 200 ºC for 2 h to make the organic matter decomposed completely then calcined at 450 ºC and 550 ºC for 6 h. The products were signed A_1 and A_2. The other was washed several times with deionized water and ethanol then calcined at 450 ºC and 550 ºC for 6 h. The products were signed C_1 and C_2. All the annealing processes were performed in air in a high temperature resistance furnace with a temperature ramp of 10 ºC/min. After aging for 5 days, the constitution of precursor was characterized by XPS. The four samples were investigated by XRD and SEM.

Characterization: X-ray diffraction (XRD) patterns were collected on a Bruker D8 advance X-ray diffractometer with CuK_α radiation. The accelerating voltage and the applied current were 40 kV and 40 mA, respectively. Data were recorded at a scanning rate of 0.02º s^{-1} in the 2θ range of 10-70º. It was used to identify the phase present and their crystallite size. The crystallite size was calculated from X-ray line broadening analysis by Scherer equation: $D = 0.89\lambda/\lambda\cos\theta$, where D is the crystal size in nm, λ is the CuK_α wavelength (0.15406 nm), β is the half-width of the peak in rad and θ is the corresponding diffraction angle. The microstructure of as-prepared sample was analyzed with the help of scanning electron microscopy (AMRAY-1000B). The size and the shapes of the particle were analyzed by transmission electron microscopy (JEM -2010).

Sensor preparation: Four sensors were fabricated by dropping the paste on the interdigital electrodes of a microhotplate. The films were about 30 μm in thickness and their resistances were about 500-2000 kΩ. Fig. 1 shows the cross-sectional schematic view and the front view of the microhotplate. The silicon-based microhotplate is embedded with a snake-like Pt heater (20 μm in width and 20 μm in spacing) and Pt interdigital electrodes (20 μm in width and 70 μm in spacing). The process of microhotplate fabrication can be found in the literature[17]. After being dried for 3 h, the gas-sensing properties of the sensors were measured.

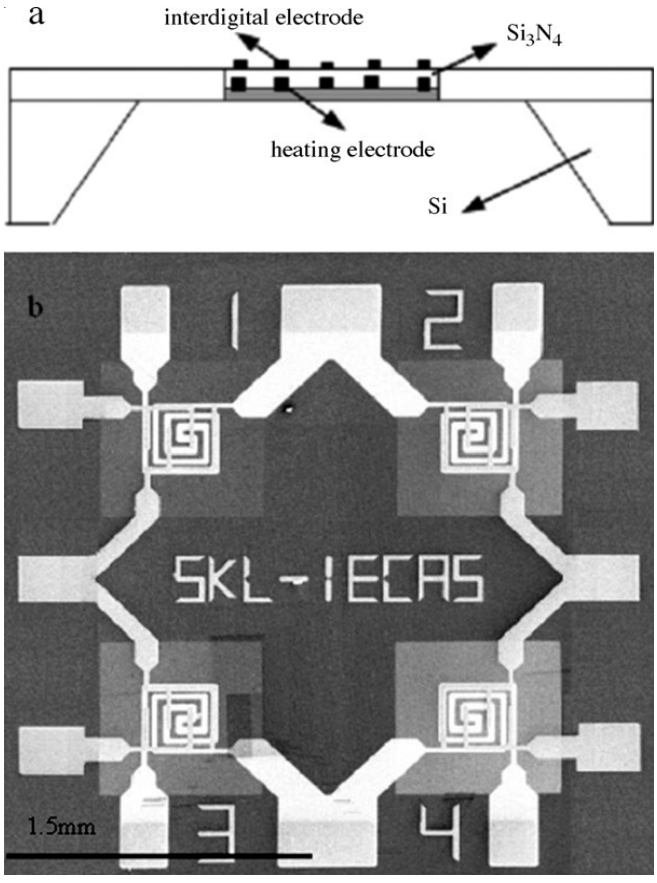

Fig. 1. (a) A cross-sectional schematic view and (b) a front view of the microhotplate

Gas sensor measurements: Gas-sensing properties were measured using a static test system, which included a test chamber (about 1 L in volume) and a data acquisition/processing system. Dry air was used as both are reference gas and a diluting gas to obtain desired concentrations of analytes. An analyte was injected into the test chamber by a syringe through a rubber plug. After the analyte was fully mixed with the diluting gas, the sensor was put into the test chamber and the response began. When the response reached a constant value, the sensor was taken out to recover in dry air. The gas response is defined as Rg/Ra, where Rg and Ra are the resistances of the sensor upon exposure to an analyte and dry air, respectively. The response time is specified as the time to rise to 90 % of the equilibrium value of sensor resistance after an analyte is injected. The recovery time is defined as the time to fall to 10 % of the final resistance value after the removal of an analyte. The operating temperature of sensors was adjusted by varying a heating voltage V_h. The experimental set-up and the schematic diagram of the measurement circuit are shown in Fig. 2.

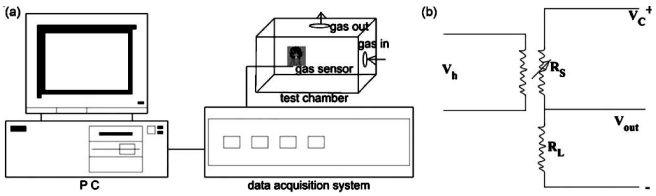

Fig. 2. (a) Experimental set-up and (b) a schematic diagram of the measurement circuit. R_L: load resistance; Rs: sensor resistance; Vc: operating circuit voltage; V_h: heating voltage; Vout: output voltage

RESULTS AND DISCUSSION

Analysis of prepared SnO_2: The XRD patterns of the as-prepared four samples of SnO_2 were shown in Fig. 3. Fig. 3 (a) showed that samples A_1 and A_2 were pure SnO_2. Fig. 3 (b) showed that samples C_1 and C_2 were SnO-doping SnO_2. The diffraction peaks of SnO assigned to (101) plane with the value of 2θ is 29.917º. It is square crystallinity with the lattice constants of a = 3.796 Å and c = 4.816 Å. Fig. 3 showed that in the samples A_1, A_2, C_1 and C_2 present SnO_2 a tetragonal rutile structure of high crystallinity and all the peaks match well with Bragg reflections of the standard rutile crystalline phase (SG: $P4_2/mnm$; JCPDS file No. 41-1445). The average crystallite size of the replicas SnO_2 were estimated according to the line width analysis of the diffraction peaks (110) based on the Scherrer formula[18,19]. It was found that the grains grew up with an increase in calcination temperature.

Fig. 4 showed the SEM images of as-prepared samples A_1, A_2, C_1 and C_2. It can be seen from Fig. 4 that A_1 and A_2 has poriferous architecture. C_1 and C_2 has floccule architecture. The aperture of A_1 and A_2 is larger than of C_1 and C_2.

Gas sensing properties: Recently, the gas sensing properties of various *n*-type semi-conductors have been widely explored[20-24]. SnO_2, which is a well-known wide-band-gap *n*-type semiconductor, shows outstanding response to NO_x, CO_x, H_2, C_2H_5OH, H_2S, *etc.*, Herein, SnO_2 based sensors were fabricated using prepared four samples A_1, A_2, C_1 and C_2 and gas sensing properties have been studied.

Fig. 5 showed the response test of four sensors of A_1, A_2, C_1 and C_2 in various gas environments, such as 50 ppm H_2S, gasoline, HCHO, Cl_2 and ethanol at the working temperature of 175 ºC. It is clearly that the sensors C_1 and C_2 are more

sensitive to these gases than A_1 and A_2 and have excellent selectivity to Cl_2 and ethanol. The sensors A_1 and A_2 almost have no response to any gas at the operating temperature of 175 ºC.

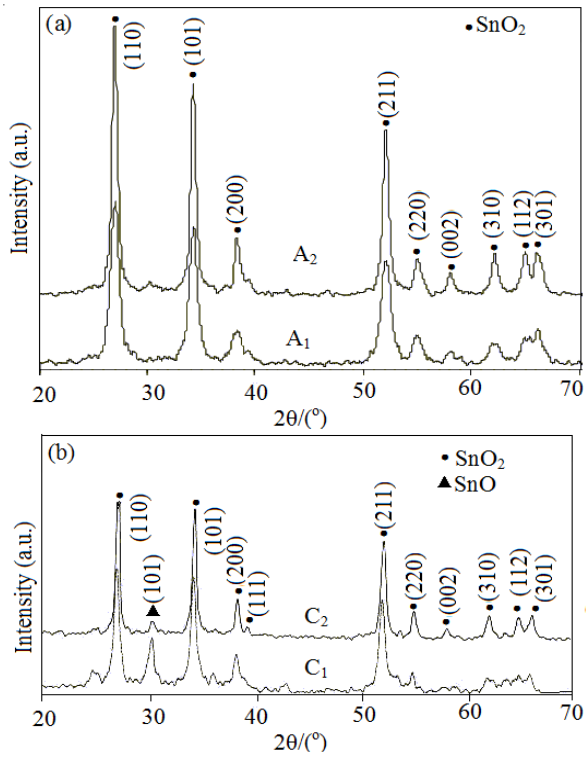

Fig. 3. XRD patterns of SnO_2: (a) A_1 and A_2 (b)C_1 and C_2

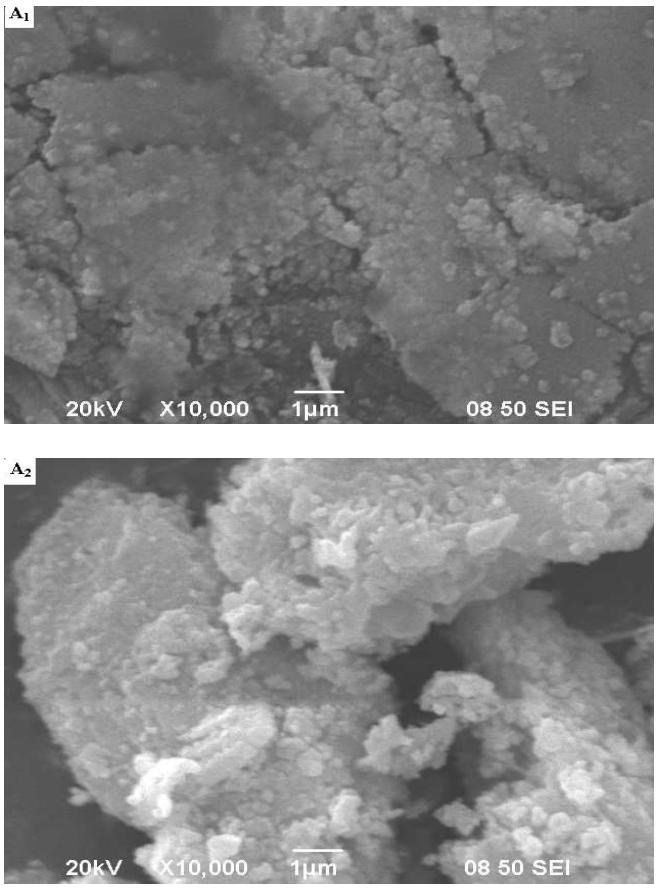

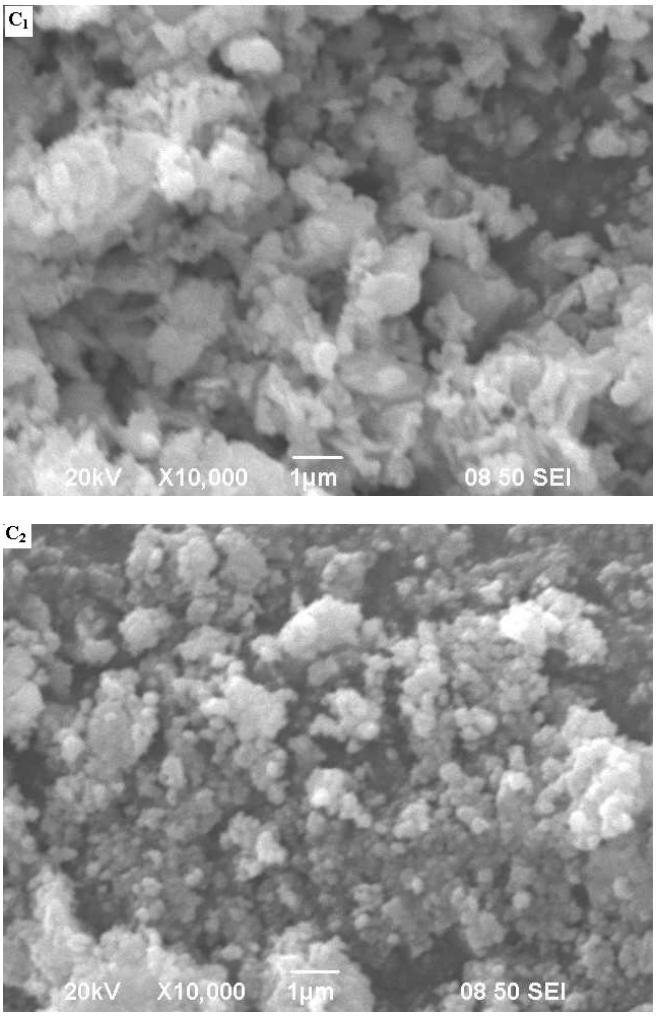

Fig. 4 SEM image of the samples A_1, A_2, C_1 and C_2

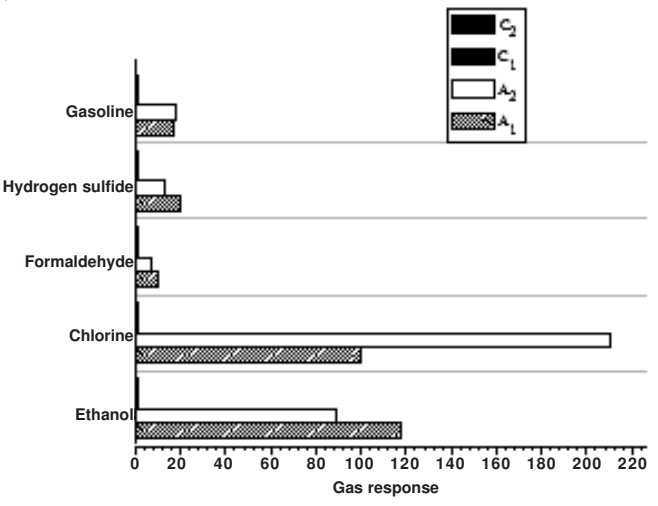

Fig. 5. Response values of A_1, A_2, C_1 and C_2 sensors to different gases of 50 ppm

Fig. 6 showed the gas sensing properties influenced by the working temperature, which is from room temperature to 300 ºC in gases of 50 ppm Cl_2 and ethanol. As we can see in Fig. 6 (a), the SnO_2-based sensors A_1 and A_2 had the maximum sensitivity to Cl_2 at 200 ºC, which were 231 and 435. Sensors C_1 and C_2 had the maximum sensitivity to Cl_2 at 300 ºC, which

were 30 and 21. Fig. 6 (b) showed the sensitivity to ethanol of A_1 and A_2 were 118 and 89. But there were almost no response to ethanol of C_1 and C_2.

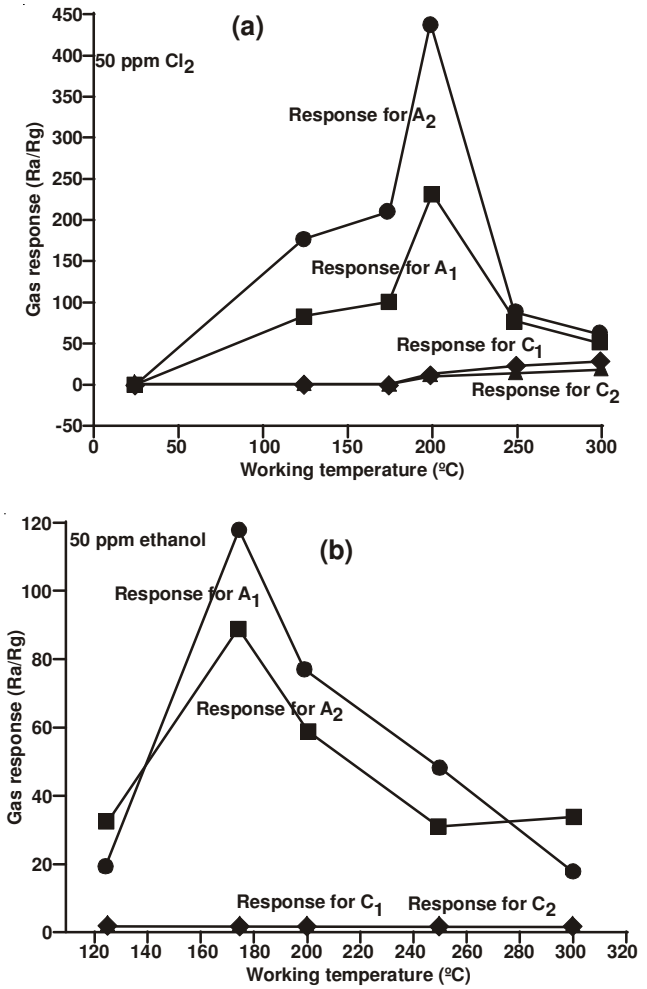

Fig. 6. Sensitivity to 50 ppm Cl_2 and ethanol at working temperature for A_1, A_2, C_1 and C_2

In an air ambience, oxygen molecules adsorb on the surface of SnO_2 and form oxygen ions (O^-, O^{2-}) by capturing electrons from the conductance band, which leads to a high resistance state of SnO_2 based sensor.

$$O_2 + e \rightarrow O_2^- \text{ (add)}$$
$$e + O_2^- \rightarrow 2O^- \text{ (add)}$$
$$e + O_2^- \rightarrow O_2^- \text{ (add)}$$

When exposed to a reducing gas, the adsorbed oxygen (O^-, O^{2-}) on the surface will react with the reducing gas, which releases electrons to the conduction band. This leads to the decreased amount of the carrier holes in the surface charge layer and the rapid increase of resistance. After the analyte is removed, the resistance returns to the original value due to the re-adsorption of oxygen.

The interaction of reducing or combustible gases with the surface chemisorbed oxygen can take place in different ways of physical or chemical reactions. Vancu *et al*. have suggested the following reaction to be favourable with the reducing gases: $R + O^- \Leftrightarrow RO + e^-$. It has also been pointed out that the gas sensing phenomenon is intimately connected with the occurrence of surface catalyzed combustion[25]. As we are aware from the catalytic chemistry, the surface acid/basic state could be advantageously utilized to favour some particular reactions. With the prior knowledge of the type of a target gas, the sensor surface could accordingly be modified in order to preferentially sense the reducing gas over other interfering gases. Based on the above theories, Gnanasekar *et al*.[26] have suggested that the following reactions would take place in the gasoline combustion on a basic surface:

$$\text{Gasoline (or LPG)} + O_2 \rightarrow CO_2 + CO + H_2O$$

Fu *et al*.[27] have suggested that aldehyde (CH_3CHO) was the intermediate product when ethanol was oxidized on the basic surface and the following reactions happened:

$$CH_3CH_2OH + O_2 \rightarrow CH_3CHO + H_2O$$
$$CH_3CHO + O^-_{ads} \rightarrow CO_2 + H_2O + e^-$$

H_2S and the chemisorbed oxygen O^- can give rise to the following reaction[28]:

$$H_2S + O^-_{ads} \rightarrow H_2O + S + e^-$$

Electrons released from the above reactions would annihilate the holes: $h\bullet + e^- \rightarrow 0$. Hence, the resistance of gas-sensing materials increased and then realized the detection of different gases. For gasoline or LPG, the population of negatively charged oxygen adsorbates effectively controls the conductance of SnO_2. For the oxide SnO_2, the electron concentration depends on the stoichiometry deviation determined by oxygen vacancies, which are predominant atomic defects. The electrical properties of nanocrystalline SnO_2 depend strongly on the surface states, produced by oxygen and other gas molecules chemisorbed at the grain boundaries, which result in the space charge appearance and band modulation. Therefore, the variation of the chemisorbed molecule density is supposed to be mainly responsible for the electrical response.

While when exposed to the oxide gases, such as Cl_2, it can be adsorbed or interact with the oxygen adsorbed onto the sensors surface according to the following reactions:

$$Cl_{2(g)} + e^- \rightarrow Cl_2^-$$
$$Cl_{2(g)} + O_2^- + 2e^- \rightarrow Cl_2^- + 2O^-$$

It is well known that ethanol can act as the reducing atmosphere and the reducing ability is stronger than formaldehyde (HCHO). So the sensitivity of nano-structured SnO_2 in this work to ethanol was higher than that to formaldehyde. Under the similar conditions, materials with higher effective surface areas such as A_1 and A_2 offer a higher probability of ethanol molecules with adsorbed oxygen and hence they are able to have a higher electrical conductivity change. The surface of C_1 and C_2 was less effective so the sensitivity were lower. On the other hand, the composition of C_1 and C_2 was different from A_1 and A_2. There was SnO phase in C_1 and C_2. It is known that SnO would react with oxygen adsorbed on the sensor surface according to the following reaction:

$$SnO + 1/2O_2 \rightarrow SnO_2$$

Therefore the concentration of oxygen ions decreased so as the resistance of SnO_2 sensors. As a result the sensitivity of A_1 and A_2 was much higher than that of C_1 and C_2.

Conclusion

Nanostructured SnO_2 has been synthesized with the method of dissolution-pyrolysis. In this paper, influence of different treatment with the precursor on SnO_2 has been studied

in detail. The precursor was treated with different methods and calcined at different temperature. SnO-doping SnO_2 was prepared from annealing the washed precursor and pure SnO_2 was synthesized from annealing the unwashed precursor. Four nanomaterials signed A_1, A_2, C_1 and C_2 were obtained. The phase, constitution and morphology of the materials are characterized by XRD and SEM. The particle size of SnO-doping SnO_2 was larger than the pure SnO_2. The gas sensing property of fabricated materials was tested. Compared to SnO-doping SnO_2, pure SnO_2 sensor shows much better gas sensing properties, which are due to larger surface area for gas adsorption and diffusion and higher concentration of oxygen ions. It is more sensitive to H_2S, Cl_2, C_2H_5OH and HCHO than SnO-doping SnO_2.

ACKNOWLEDGEMENTS

The author appreciated the financial supports from Technologies Research Funds of Luoyang Institute of Science and Technology (2008QZ21).

REFERENCES

1. J.M. Wu and C.H. Kuo, *Thin Solid Films*, **517**, 3870 (2009).
2. H.-X. Zhang, C. Feng, Y.-C. Zhai, K.-L. Jiang, Q.-Q. Li and S.-S. Fan, *Adv. Mater*., **21**, 2299 (2009).
3. I.-S. Hwang, J.-K. Choi, S.-J. Kim, K.-Y. Dong, J.-H. Kwon, B.-K. Ju and J.-H. Lee, *Sens. Actuators B,* **142**, 105 (2009).
4. A.Z. Adamyan, Z.N. Adamyan and V.M. Aroutiounian, *Int. J. Hydrogen Energy*, **34**, 8438 (2009).
5. L. Ottaviano, M. Kwoka, F. Bisti, P. Parisse, V. Grossi, S. Santucci and J. Szuber, *Thin Solid Films*, **517**, 6161 (2009).
6. F. Suzanne, Z. Arie and B.A. Gregg, *J. Phys. Chem. B*, **101**, 4490 (1997).
7. R. Khan and T.J. Kim, *J. Hazard. Mater.*, **16**, 1179 (2009).
8. F. Cheng, Z. Tao, J. Liang and J. Chen, *Chem. Mater*., **20**, 667 (2008).
9. E. Li, Z.X. Cheng, J.Q. Xu, Q.Y. Pan, W.J. Yu and Y.L. Chu, *Cryst. Growth Des*., **9**, 2146 (2009).
10. F. Gu, S.F. Wang, M.K. Lü, G.J. Zhou, D. Xu and D.R. Yuan *J. Phys. Chem. B,* **108**, 8119 (2004).
11. Z. Remes, M. Vanecek, H.M. Yates, P. Evans and D.W. Sheel, *Thin Solid Films,* **517**, 6287 (2009).
12. H.T. Feng, R.F. Zhuo, J.T. Chen, D. Yan, J.J. Feng, H.J. Li, S. Cheng and P.X.Yan, *Physica E,* **41**, 1640 (2009).
13. S. Das, S. Chaudhuri and S. Maji, *J. Phys. Chem. C*, **112**, 6213 (2008).
14. H.C. Chiu and C.S. Yeh, *J. Phys. Chem. C*, **111**, 7256 (2007).
15. V. Subramanian, W.W. Bruck, H.W. Zhu and B.Q. Wei, *J. Phys. Chem. C*, **112**, 4550 (2008).
16. X.D. Lou, C.Y. Peng, X.B, Wang and W.F. Chu, *Vacuum*, **81**, 883 (2007).
17. X.L. He, J.P. Li, X.G. Gao and Li Wang, *Sens. Actuators B,* **93**, 463 (2003).
18. C. Wagner and G. Muilnberg, Handbook of X-ray Photoelectron Spectroscopy, Physical Electronics Division; Perkin-Elmer Corp., Eden Prairie, MN, (1979).
19. A. Gurlo, N. Barsan, U. Weimar, M. Ivanovskaya, A. Taurino and P. Siciliano, *Chem. Mater*., **15**, 4377 (2003).
20. Q. Dong, H.L. Su, J.Q. Xu and D. Zhang, *Sens. Actuators B*, **123**, 420 (2007).
21. H. Huang, O.K. Tan, O.K. Tan, Y.C. Lee, M.S. Tse, J. Guo and T. White, *Nanotechnology*, **17**, 3668 (2006).
22. V.V. Sysoev, B.K. Button, K. Wepsiec, S. Dmitriev and A. Kolmakov, *Nano Lett.*, **6**, 1584 (2006).
23. T. Hyodo, K. Sasahara, Y. Shimizu and M. Egashira, *Sens. Actuators B,* **106**, 580 (2005).
24. N.S. Ramgir, I.S. Mulla and K.P. Vijayamohanan, *Sens, Actuators B,* **107**, 708 (2005).
25. S.R. Morrison, *Sens. Actuators B*, **12**, 425 (1987).
26. K.I. Gnanasekar, V. Jayaraman, E. Prabhu, T. Gnanasekaran and G. Periaswami, *Sens. Actuators*, *B*, **55**, 170 (1999).
27. M.G. Fu, X.J. Wang, J. Chen, H.Y. Wang and J. Zhengzhou, *Inst. Light Ind*., **28**, 160 (1994).
28. G.J. Fang, Z.L. Liu and Z.C. Zhang, *J. Chin. Rare Earth Soc*., **15**, 10 (1997).